Experiments in Fluids manuscript No.
(will be inserted by the editor)

The potential of on-line optical flow measurement in the control and monitoring of pilot-scale oxy-coal flames

Pal Toth · Zhonghua Zhan · Zhisong Fu · Arpad B. Palotas · Eric G. Eddings · Terry A. Ring

Received: date / Accepted: date

Abstract Digital image processing techniques offer a wide array of tools capable of extracting apparent displacement or velocity information from sequences of images of moving objects. Optical flow algorithms have been widely used in areas such as traffic monitoring and surveillance. The knowledge of instantaneous apparent flame velocities (however they are defined) may prove to be valuable during the operation and control of industrial-scale burners. Optical diagnostics techniques, coupled with on-line image processing have been applied in the optimization of coal-fired power plants; however, regardless of the available technology, the current methods do not apply optical flow measurement. Some optical flow algorithms have the potential of real-time applicability and are thus possible candidates for on-line apparent flame velocity extraction. In this paper, the potential of optical flow measurement in on-line flame monitoring and control is explored.

Keywords Burner control · Pulverized coal flame · Flame velocity · Oxy-coal firing · Optical flow

1 Introduction

The applicability of digital image processing-based techniques for monitoring, controlling and optimizing industrial-scale pulverized coal burners has been widely studied. Digital imaging is an attractive approach to achieve these objectives because of its flexibility and high data rate. Previous studies managed to obtain information regarding flame luminosity or brightness (Shimoda et al 1990; Lu et al 2004, 2005), temperature, based on two-color pyrometric concepts (Jiang et al 2009; Smart et al 2010; Xiangyu et al 2011; Lou et al 2011; Gonzalez-Cencerrado et al 2012), flame geometry (Baldini et al 2000), flame stability and flicker frequency (Zhang et al 2011; Sun et al 2011; Gonzalez-Cencerrado et al 2012) and flame spectra (Baeg et al 2005; Sun et al 2011), among others. The key incentive behind advanced, vision-based on-line flame monitoring are the "increasingly stringent standards on energy saving and pollutant emission" (Lu et al 2005). Water (Lu et al 2004; Gonzalez-Cencerrado et al 2012) or air-cooled (Jiang et al 2009; Lou et al 2011), ruggedized camera assemblies with optical guides have been used for flame monitoring in systems larger than laboratory-scale.

Optical flow is a general term referring to the apparent (projected) motion of brightness patterns in a sequence of scalar (intensity) images. Computer algorithms that can extract optical flow (OF) from video data are used in off-line combustion diagnostics, such as in particle image velocimetry (PIV) or particle tracking velocimetry (PTV). By the term "off-line" we refer to the typical procedure by which combustion diagnostics are performed: the imaging is done prior to the batch-processing of image data. In contrast, by "on-line" measurements we refer to techniques that can provide information simultaneously with imaging at a sufficient data rate so that the extracted information can be used a in control loop.

Pal Toth
Department of Chemical Engineering, University of Utah, 50 S. Central Campus Drive, Salt Lake City, UT 84112-9203
Tel.: +801-581-6915
E-mail: pal.toth@utah.edu

UU IR Author Manuscript

In an industrial environment, typical optical combustion diagnostics methods are rarely applied because of their sensitivity to dust, vibrations, temperature and due to their equipment cost. Although efficient software allows for on-line data acquisition (Arik and Carr 1997; Roberts 2012) in industrial settings, the standard method for flow visualization and velocity measurement, PIV, is impractical due to the need to operate lasers. In PIV, lasers are used to make velocity measurements planar; i.e., motion only in the plane of the illuminating laser sheet is registered. By omitting the use of laser sheets, the acquired flame image sequences contain out-of-plane motion as well. Nevertheless, this motion, if extracted, might prove to be useful information from the perspective of flame monitoring and control. None of the previously listed studies (Kurihara et al 1986; Baek et al 2001; Lu et al 2008) apply optical flow extraction.

In contrast with the typical cross-correlation based PIV algorithms, optical flow algorithms extract apparent motion based on the brightness constancy assumption, expressed as

$$I(x, y, t) = I(x + u, y + v, t + 1), \tag{1}$$

where $I(x, y, t)$ is the intensity in an image sequence at a pixel location (x, y) and time t and (u, v) are the two components of the apparent displacement. Note that for notation purposes, the interframe time Δt is chosen to be unity, but when computing OF velocity, (u, v) must be divided by the real value of Δt. Optical flow algorithms aim to solve the inverse problem of obtaining (u, v) by satisfying Equation (1). More refined methods apply multi-scale frameworks (Bouguet 2000), image segmentation (Farneback 2001), approaches that can handle discontinuous flow fields (Deriche et al 1995) or balance the resulting flow to also account for the gradient constancy assumption:

$$\nabla I(x, y, t) = \nabla I(x + u, y + v, t + 1) \tag{2}$$

Similar algorithms were used to perform unseeded, planar, laser velocimetry on small-scale flames (Fielding and Long 2000; Fielding et al 2001) or to study mixture formation (Scholz et al 2008).

The optical flow algorithm implemented in this study (Brox et al 2004) solves Equations (1) and (2) by minimizing the energy functional

$$E(\mathbf{w}) = E_{data} + \alpha E_{smooth}, \tag{3}$$

where

$$E_{data}(\mathbf{w}) = \int_{\Omega} \left(|I(\mathbf{x} + \mathbf{w}) - I(\mathbf{x})|^2 + \gamma \, |\nabla I(\mathbf{x} + \mathbf{w}) - \nabla I(\mathbf{x})|^2 \right) \mathrm{d}\mathbf{x} \tag{4}$$

$$E_{smooth}(u, v) = \int_{\Omega} \psi \left(|\nabla_3 u|^2 + |\nabla_3 v|^2 \right) \mathrm{d}\mathbf{x} \tag{5}$$

Here, $\psi(s^2) = \sqrt{s^2 + \epsilon}$, with ϵ being set to 0.001, $\nabla_3 = (\partial_x, \partial_y, \partial_t)^{T\,1}$ is the spatio-temporal intensity gradient, $\mathbf{w} = (u, v, 1)^T$ is the vector of interframe displacement, $\mathbf{x} = (x, y, t)^T$ is the vector of spatio-temporal location in the video, Ω is a local image region and the parameters γ and α are free parameters. The parameter γ is the relative importance of the gradient constancy assumption in solving the inverse problem and α is the importance of the smoothness criterion of the OF velocity field $\mathbf{w}$. The algorithm of Brox et al. was chosen due to its high accuracy and computational efficiency.

In this paper, the potential of an optical flow velocimetry (OFV) technique that does not require seeding particles or lasers, that can operate at safe distances from a pulverized-coal flame and that can be made efficient enough for on-line data acquisition in flame monitoring and control is demonstrated. An oxy-coal flame with a nominal thermal output of 120 kW was studied by the OFV method. The responsiveness and sensitivity of OFV measurements is demonstrated by monitoring changes in OF velocities following perturbations in combustion conditions.

2 Materials and methods

In this section, the relevant details of the experiments are presented. This section includes a description of the combustion system, imaging equipment and image processing.

[1] T denotes vector transpose

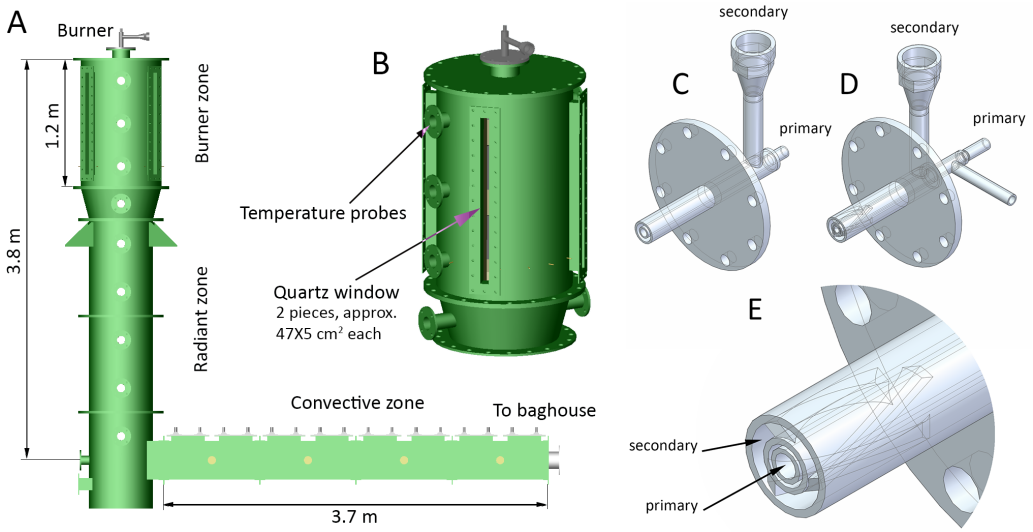

Fig. 1 A schematic of the combustion system used in the experiments. A - side view of the oxy-coal combustor with the combustion chamber and flue-gas disposal system. B - a rendering of the combustion chamber. C - a rendering of the co-axial burner. D - a rendering of the swirl burner. E - a close-up view of the head of the swirl burner with the swirling vanes in the secondary stream shown. The middle stream of the swirl burner was not used.

2.1 The combustion system

The combustion system used in this study was a pilot-scale oxy-coal combustor burning Utah Sufco bituminous coal with a nominal heat output of 120 kW. Oxy-firing is a promising new technology with the objective of reducing global CO_2 emissions by facilitating the more complete capture of flue gas CO_2. In oxy-coal firing, coal is fired in a stream of relatively pure O_2 with CO_2 that has been recycled from the combustion products (Buhre et al 2005). In these experiments, pure CO_2 was utilized without flue gas recycle.

The details of the construction of the oxy-coal combustor have been reported previously (Zhang et al 2007). In brief, the combustion system consists of a refractory-lined, cylindrical combustion chamber with an inner diameter of 0.61 m, a cylindrical radiative section with an inner diameter of 0.27 m and a convective zone with installed heat exchangers (0.15×0.15 m, square cross-section). The flue gas leaving the convective zone passes through a bag filter before being emitted. The furnace is controlled by an automated digital system that takes gas concentration, flow rate and temperature information as the input in its control loop. The combustion chamber ("burner section") of the system has built-in electric wall heaters (each 800 W) that allow for keeping wall temperature constant during experiments. This section also has 4 quartz windows set at 90 degree orientations (approximately 5×100 cm^2) as optical access ports. Figure 1A and Figure 1B show the combustion system schematically.

Two types of burners were used in the experiments: a co-axial zero-swirl burner and a swirl burner. Both burners were tube-in-a-tube constructions (with pulverized coal and the primary gas stream in the inner tube and the secondary gas stream in the outer annulus). The two types of burners produced significantly different flame geometries. From the perspective of computing optical flow from flame images, the co-axial burner was expected to produce flames with more homogeneous velocity fields dominated by the axial velocity component, while the swirl burner was thought to produce flames with a wider range of arising instantanaeous velocities and higher tangential velocities. For this reason, we chose to evaluate the optical flow method with both types of burners. The dimensions of the burners can be seen in Table 1. Isometric views of the burners are shown in Figure 1C-E.

2.2 Imaging

A Photron APS-RX type visible, high-speed camera was used to acquire most of the flame image sequences presented in this paper. The camera captured 1 Mpixel, grayscale images at a bit depth of 10 bits. A

Table 1 Burner dimensions, mm (ID - inner diameter, OD - outer diameter)

	Inner tube ID	Inner tube OD	Outer tube ID	Outer tube OD	Remarks
Co-axial burner	15.8	21.34	35.05	42.16	-
Swirl burner	12.52	26.67	40.89	48.26	3 turning vanes, 15°

telephoto lens (Tamron, 18-270 mm) was used in conjunction with the camera. The focal length of the camera was set to 50 mm. The spectral sensitivity range of the camera was 300-700 nm. The magnification of the system was approximately 0.05. The overall lateral resolution of the system was approximately 2 mm in the center plane of the imaged flame, at a standoff of 1.5 m from the quartz window.

The camera captured a field of view (FOV) of approximately 50×50 cm^2. This FOV contained about half of the total height of the quartz window. The whole window was not captured in order to obtain sufficient image resolution over the flame image. The region 0-50 cm downstream of the burner was captured in cases where the co-axial burner was used, while the region approximately 10-60 cm downstream of the burner was imaged in the cases done with the swirl burner. This choice of regions of interest is justified by the different flame liftoff for the two burners: flames produced by the co-axial burner were usually attached to the burner surface, while swirled flames were detached and their luminous region started downstream of the burner. Each recording was approximately 5 minutes long. As the luminous intensities of the flames produced by the two burners were different, the aperture setting of the lens was set to best fit the dynamic range of the camera. In every case, the entire thickness of the flame was within the zone of acceptable sharpness. Imaging parameters during runs were not changed.

The camera was triggered such that the timing simulated the double-framing mode of typical PIV cameras. In this timing scheme, frames are acquired in pairs and the time between subsequent pairs is longer than the time between frames within pairs. The interframe time between frames within pairs for the camera was 333 µs. Fifty frame pairs were acquired each second. The integration time of each frame was 80 µs.

For triggering the camera, a Stanford Research DG535 type digital delay generator was used. The generatated TTL pulses were 1 µs long. Each pulse reset the internal clocks of the camera. The second frames in dual-frame pairs were triggered by the reset 3 kHz internal frequency generator, thus the interframe time of 333 µs was realized inside dual-frame pairs.

2.3 Image processing

In the first step of image processing, the acquired images were registered. The registration step included cropping and rotating the images to a vertical orientation; i.e., the burner axis pointed downwards.

The processing of the OFV images utilized the optical flow algorithm of Brox et al. (Brox et al 2004). There was no preliminary normalization necessary before running the optical flow routine on the acquired luminosity images. A standard library (OpenCV) was used to implement the CUDA variant of the OFV routine on a graphical processing unit (GPU). There are a number of free parameters in this algorithm (see Section 1).

Omitting further details, one needs to set a high value of α when the underlying displacement field is assumed to be smooth, a high value of γ when one wants to balance the extracted motion field to favor edges over brightness patterns in tracking and a high value of n_p when a large spatial variation of displacement is expected. Increasing both n_i and n_o typically results in higher precision at the cost of increased computation time. In our implementation, the remaining parameter, r_f, was used in conjunction with n_p for fully determining the image pyramid. For computing the OF velocity fields presented in Section 3 and Section 4.3, the following parameter values were used: $\alpha = 100$, $\gamma = 3$, $\eta = 0.5$, $n_p = 2$, $n_i = 7$, $n_o = 50$[2]. The parameters were set by inspecting the obtained displacement fields and visually comparing them to overlaid double frames. An example of overlaid frames and extracted displacement fields are shown in Figure 2.

[2] These parameter values are consistent with the original paper of Brox et al. (Brox et al 2004). η is the reduction factor between subsequent pyramid levels.

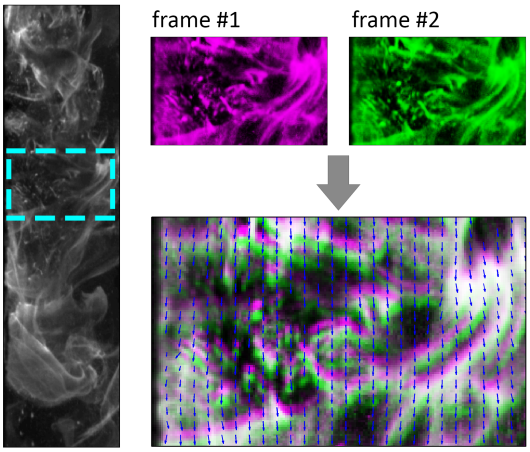

Fig. 2 An example OF velocity field obtained from a frame pair. Left: frame #1 of a flame image pair. The rectangle shows a detail that was enlarged. Top right: the marked detail in frames #1 (magenta) and #2 (green). Bottom right: overlaid frames and extracted displacement field. The purpose of this montage is to illustrate how the flame image moves between two consecutive frames. The images were contrast-enhanced to improve visibility.

Note that the spatio-temporal gradient (see Equation (5)) was replaced with the spatial gradient, since the two-frame implementation of the optical flow algorithm was used. The spatial gradient was computed by the Sobel-operator on every scale of the image pyramid (Gonzalez and Woods 2001).

3 Flame monitoring by OFV

In this section, the potential of OFV in practical applications as an input provider for control loops is demonstrated. In these tests, image sequences were produced that captured transient flame behavior during scenarios in which furnace operating conditions were abrupty changed. These sequences of images were processed by the OFV algorithm and transient OF velocity maps were computed.

The test scenarios simulated unexpected pressure fluctuations in the secondary gas inlet stream and abrupt changes in the coal feeding rate. Each of these scenarios started from the same base conditions, which were altered during operation and the transient behavior of the flame was captured by the OFV technique. By these scenarios, we studied the effect of decreasing or increasing the secondary CO_2 flow and decreasing the coal feed rate. A total of 6 runs were done: the three test scenarios (CO_2 drop, CO_2 increase and coal feed rate decrease) were run with both the co-axial and swirl burners. The absolute change in the total gas flow rate studied during the scenarios was approximately 15%, while the decrease in coal feed rate was about 40%.

The operating conditions are shown in Table 2. Characteristic flame images shown in Figure 3 illustrate the visible changes caused by the perturbations. As can be seen, changing the operating conditions altered flame appearance in every case. The most drastic changes were caused by decreasing the coal feed rate, which de-stabilized the flames and resulted in a flickering behavior.

The simplest way to illustrate the velocity tracking capabilities of the OFV method is the visualization of the transient OF velocity. Since the visualization of transient two-dimensional fields is difficult, it is practical to present results as transient point measurements. Note that OFV is capable of extracting velocities within the whole region of interest, thus reducing the data to point measurements involves defining "points", in which OF velocity magnitude is tracked as a simple scalar parameter. Figure 4 serves to illustrate this concept. The "point measurements" shown in Figure 4 are in fact spatial averages of OF velocity magnitude within small interrogation areas defined within image frames. These small subregions are shown as green (position #1, far-burner) and blue (position #2, near-burner) rectangles. The interrogation areas were approximately 0.4 and 0.2 m downstream of the burner for the runs done with the co-axial burner. The camera was repositioned for runs with the swirl burner to best capture the luminous zones of the swirled flames. For those runs, the interrogaton areas were placed at approximately 0.5 and 0.3 m downstream of the burner.

Table 2 Operating conditions during the test scenarios. The table lists three different scenarios. These three scenarios were run with both the co-axial and swirl burners, thus the total number of experiments run was 6. Arrows denote the abruptly changed parameters from base operation. The base settings were the same in each scenario.

Parameter	Unit	CO_2 flow rate drop	CO_2 flow rate rise	Coal flow rate drop
Coal feed rate	kg/h	4.7	4.7	4.7→2.7
Primary O_2	kg/h	1.1	1.1	1.1
Primary CO_2	kg/h	6.8	6.8	6.8
Secondary O_2	kg/h	10.4	10.4	10.4
Secondary CO_2	kg/h	10.4→5.9	10.4→14.9	10.4
Wall temperature	°C	1010	1010	1010
Flue gas exit temperature	°C	200	200	200
Flue gas O_2 concentration	vol%	3→varying	3→varying	3→varying

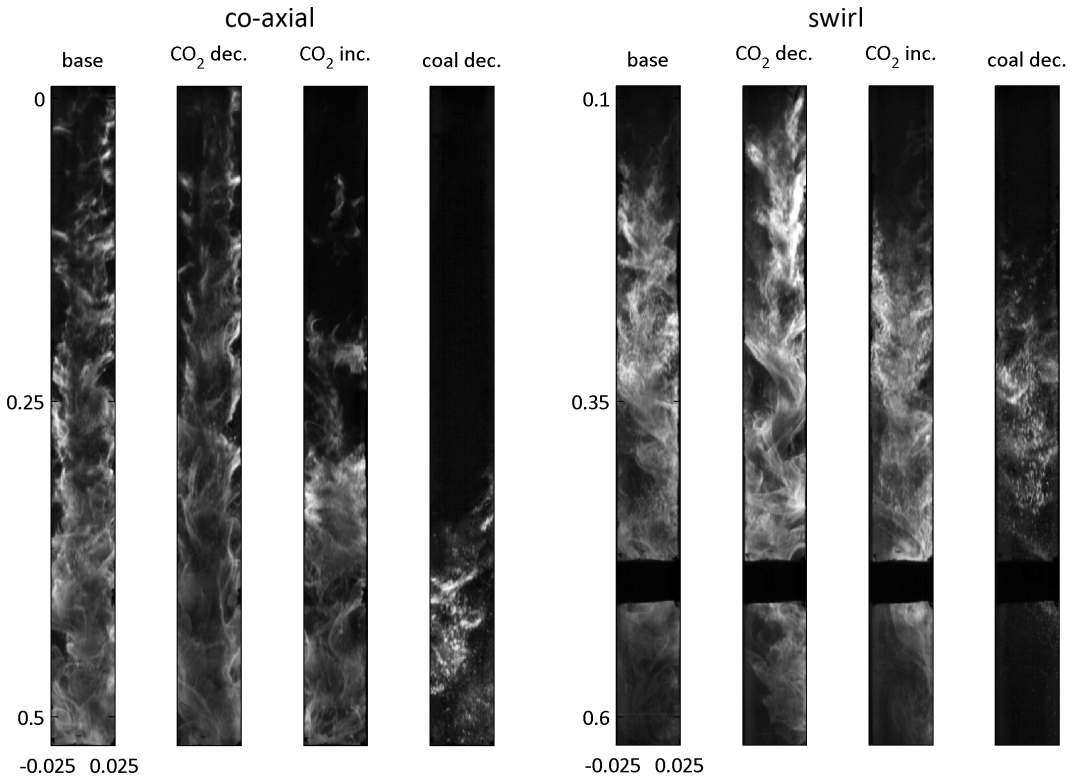

Fig. 3 Characteristic flame images of the different experimental cases. The differences in appearance are caused by changing aerodynamic, chemical and thermal conditions. The images were slightly contrast-enhanced to improve visibility. Intensities are normalized (Pizer et al 1987). The dimensions are in meters. The gaps in the swirled flame images are gaps between the two parts of the quartz window.

As seen in Figure 4, the obtained OFV velocities were responsive to changes in operating conditions. In the first test scenario shown in Figure 4, the flow rate of secondary CO_2 was decreased by 15%. Shortly after the transient event, OFV indicated a drop of apparent velocity in both interrogation areas. The measurements of the flue gas analyzers slowly followed the trend detected by OFV. The time lag between the optical method and the gas analyzers was approximately 2 minutes. Note that this time lag was due to the travel time of the sampled gas from the combustor to the flue gas analyzers installed in a control room. The length of the gas transport tubes was on the order of 10 m. Even with this time delay subtracted, the flue gas analyzers showed a much slower response (around 3 minutes) in terms of reaching the new steady state. This slow response is specific to the gas analyzers that were used; however, the response time reported here most likely well represents the expected responsiveness of conventional gas analyzers. In the test in which the secondary CO_2 was decreased, apparent velocity most likely decreased due to reduced volumetric

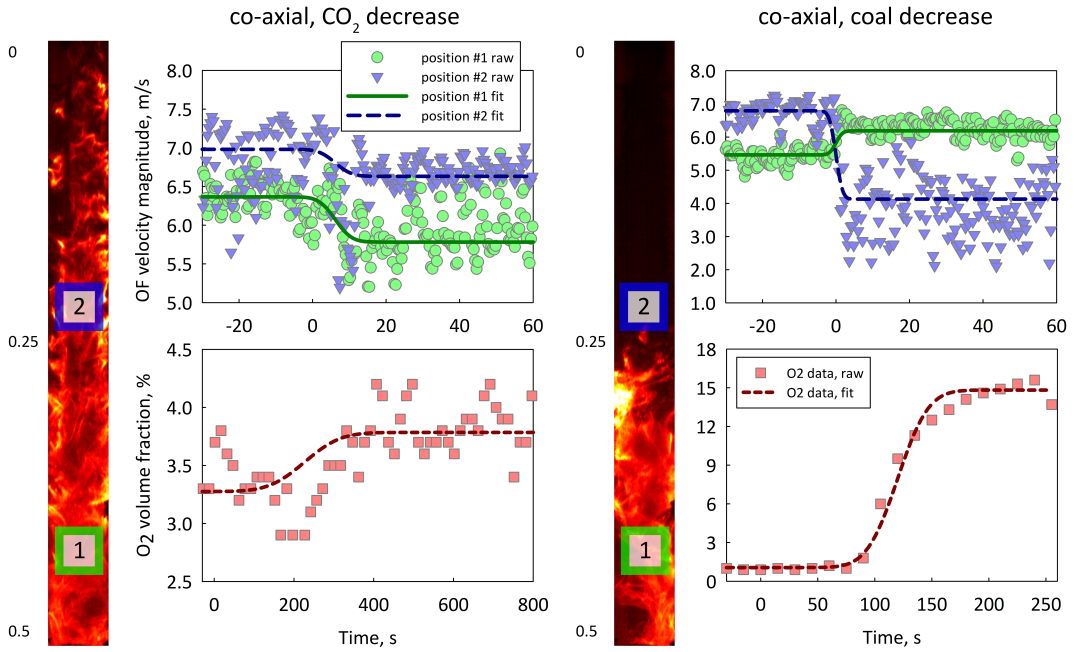

Fig. 4 A demonstration of transient OF velocity magnitudes measured during two scenarios: decreasing CO_2 and decreasing coal feed rate. Both tests were done with the co-axial burner. The flame images show the locations of subregions in which the displayed transient velocities were measured and illustrate flame detachment. Axial coordinates are given in meters. The top row shows the OF velocity measurements collected within the two subregions. Note that the shown raw OF velocity data are subsampled to improve visibility - the original measurements produced 50 velocity maps per second. The bottom row shows the response in the O_2 concentration of the flue gas, measured by infrared gas analyzers. The first column shows the data collected during the CO_2 drop scenario and the second column shows results of the coal decrease scenario. Trend lines are best fits of the generalized logistic function (Richards 1959) computed by nonlinear regression. The time scale shown has the origin at the transient event; i.e., at the instant when the operating conditions were changed. The time delay in the gas analyzer system was not subtracted from the x-axis coordinates in figures of the bottom row in order to illustrate the typical delay of gas analyzers compared to OFV measurements.

gas flow. Flame stability was not affected by this change. Flue gas O_2 concentration increased due to the reduced dilution of the flue gas by CO_2.

Interpreting the results shown in the second column of Figure 4 is more difficult as flame stability was significantly affected by decreasing the coal feed rate. Under such conditions, the interpretation of the results is only possible by considering thermal, chemical and aerodynamic effects simultaneously. The high rise in flue gas O_2 concentration was caused by the massively changed stoichiometric ratio in the flame. The decreased velocities measured in position #2 (closer to the burner head) showed significantly increased variation and reduced data rate. The change in data rate was caused by flame detachment - in other words, the luminous zone of the flame shifted downstream, away from the burner surface. Flickering flame behavior may cause insufficient luminosity at certain instances in the interrogated area, which in turn results in missing OFV data. The change of mean OF velocity in both positions was possibly caused by the downstream shifting of the ignition and devolatilization zones of the flame. In these zones, due to high rate of heat generation and the release and expansion of volatiles, flame velocity is expected to have a local maximum.

Figure 5 shows the transient velocities obtained in the rest of the transient test scenarios. In most cases, OFV produced useful responses in the transient apparent velocity signals. In some cases, e.g., in the case of decreasing CO_2 with the swirl burner, even the oscillatory behavior of velocity caused by the abrupt change in flow rates was captured. Note that some trends are not obvious in Figure 5, such as the increasing velocities that followed the decrease in the secondary CO_2 in the case of the swirl flame. For a satisfying explanation of this observation, it is useful to study the joint behavior of apparent flame velocity and intensity. Further trends seen in Figure 5 are explained in conjunction with the joint intensity-velocity data. Figure 6 shows extracted axial profiles of flame intensity and OF velocity magnitude. The presented profiles are ensemble-averages of the two "steady" states in each experiment: the base starting operation

UU IR Author Manuscript

and the operation after the varied parameter was changed. Note that by steady states we simply refer to the operation before and after the perturbation - by this term, we do not intend to characterize the "steadiness" of each state, as in some cases (e.g., the coal flow rate drop scenarios), the flame remained unstable after the transient event.

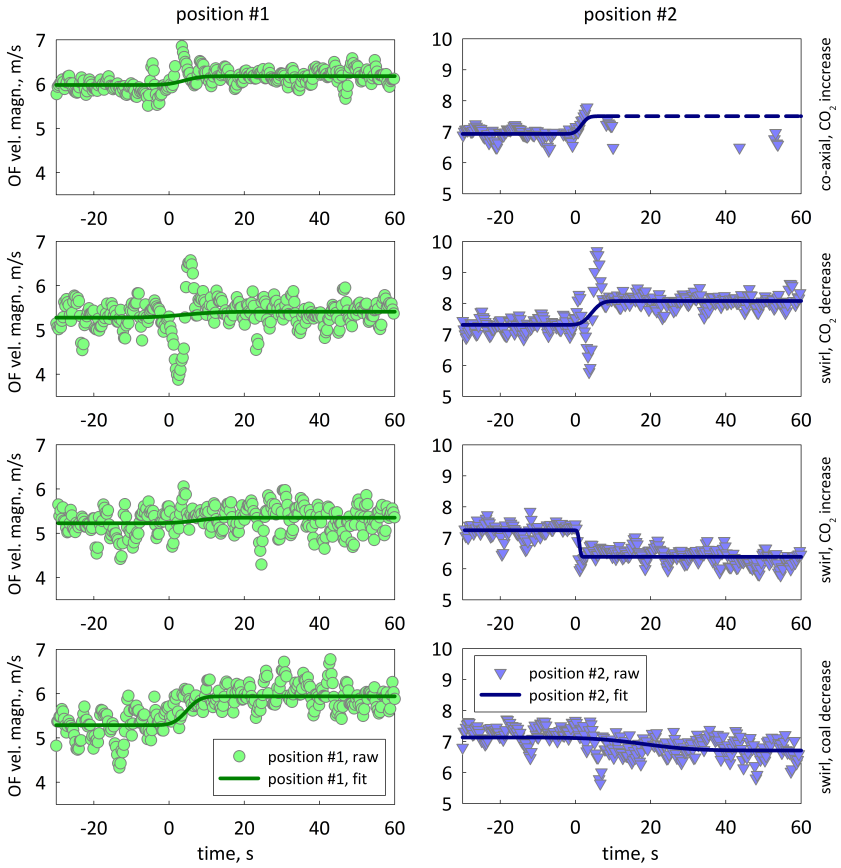

Fig. 5 Transient time-apparent velocity plots showing the response in OF velocity values obtained by OFV to changes in operating conditions. The horizontal axis shows time in seconds, the vertical axis is OF velocity magnitude in m/s. Labels indicate the interrogated subregion in the flame and the test scenarios. Fit functions are of the logistic form.

As mentioned previously, decreasing the CO_2 co-flow in the flames produced by the co-axial burner decreased OF velocity magnitudes in most of the observed region of interest. This can be explained by the lower volumetric flow rate of gas. At the same time, as seen in Figure 6, flame intensity increased, possibly due to the decreased amount of diluting CO_2. In the case of the co-axial burner, increasing CO_2 co-flow did not clearly produce the opposite effect, as this change destabilized the flame. For this reason, OF velocity and intensity data were only available in the lower portion of the imaged region (below 0.25 m downstream from the burner). In this region, apparent flame velocity showed an increasing trend with axial location and the perturbed OF velocity exceeded the base velocity at approximately 0.4 m downstream of the burner. The low OF velocity in more upstream regions of the flame was due to flame detachment. A similar trend is seen in the scenario in which coal feed rate was decreased, indicating that in both cases, the co-axial burner produced a detached flame. Notice the higher variance in both apparent flame velocity and intensity in this scenario, which suggests an unstable flame.

The scenarios varying CO_2 co-flow with the swirl burner are illustrative of the joint effect of thermal, chemical and aerodynamic factors. With the swirl burner, in contrast with the co-axial cases, decreasing CO_2 increased both velocities and flame intensity, while increasing CO_2 co-flow decreased them. The trends in flame intensity profiles can be explained by thermal and chemical principles. Decreasing CO_2 flow rate decreases the dilution of the flame, which affects the total thermal inertia of the flame, possibly along

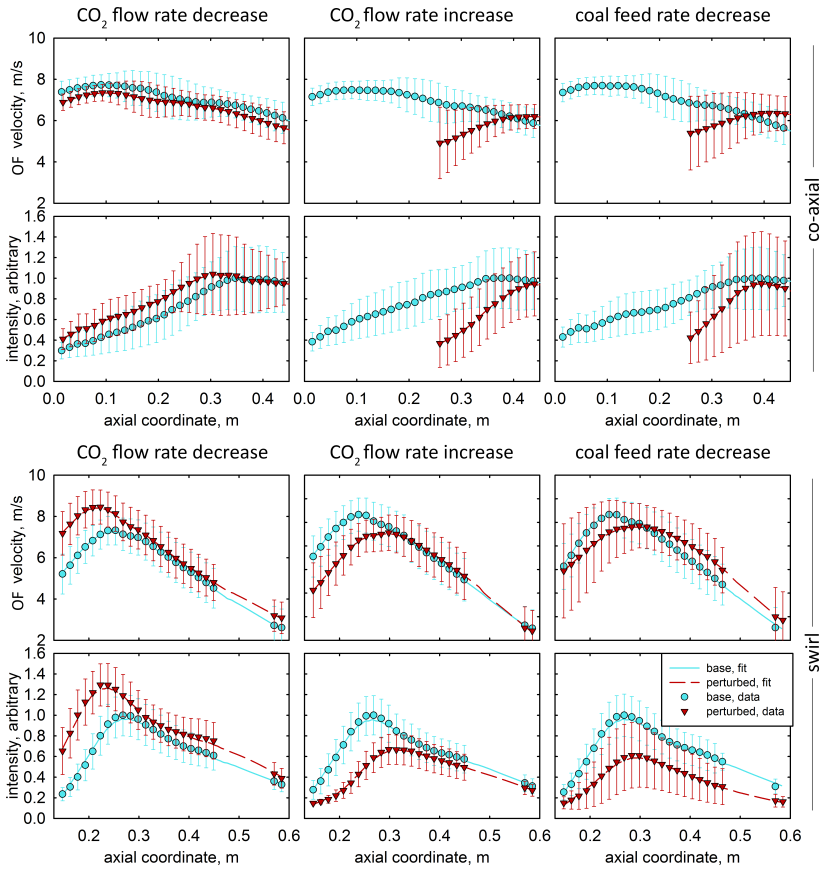

Fig. 6 Extracted axial profiles of apparent flame velocity magnitude and intensity. The profiles are ensemble-averages of "base" and "perturbed" operation. The averages were computed in subsets before and after the transient events. The errorbars indicate one standard deviation of the collected measurements. Top row: OF velocity profiles of the cases run with the co-axial burner. Second row from the top: flame intensity profiles of flames produced by the co-axial burner. Third row: OF velocity profiles of the cases run with the swirl burner. Second row from the top: flame intensity profiles of flames produced by the swirl burner. The gaps in the swirl case profiles were caused by the blocked optical access between the two parts of the quartz window. Trendlines and interpolation over missing data were computed by the LOESS method (Cleveland 1979).

with reaction rates. Trends in OF velocity profiles are more difficult to interpret, due to the significance of aerodynamic factors. Referring back to part E of Figure 1, the varied CO_2 flow rate affects only the secondary stream of the swirl burner - this is the swirled stream. Therefore, if the the momenta of the secondary and primary streams are comparable (they were in these cases), it is expected that changing the flow in the secondary stream affects the overall swirl of the flame. When flow rate is increased in the secondary stream, a higher tangential velocity is attained throughout the flame, which increases the jet-like spread of the flame, resulting in lower velocity magnitudes. This is a possible explanation for the reversed trends in OF velocity in the swirled flames relative to the zero-swirl flames seen in Figures 6 and 5. Further proof is provided for this idea in Figure 7. In the coal decreasing scenario, the swirl flame also showed an unstable behavior - this is visible in the high variation of OF velocity in regions above 0.3 m downstream of the burner (this is the zone of detachment) and in the high variation of intensity values. The shifted OF velocity profile is also indicative of downstream shifted ignition and devolatilization zones. Due to the significantly reduced thermal output of the flame, intensity decreased over the whole imaged area compared to the base state.

Apart from apparent velocity magnitude, the direction information in the extracted OF velocity fields can also be considered for utilization in control loops. The direction of apparent velocity vectors itself lacks generality for direct use, but a scalar property characterizing the directions in the vector fields can be a

useful candidate. Such a scalar property can be a measure analogous to the swirl number of a flame The swirl number is defined as

$$S = \frac{\int_0^R wurdr}{\int_0^R uurdr}, \tag{6}$$

where w and u are tangential and axial velocity components, respectively, r is the radial coordinate and R is some characteristic radius of the system. Customarily, S is computed by using mean velocities and burner geometries, but it can also be computed locally, using local means of velocity. Unfortunately, r is not measured by the OFV method; thus, the local version of S cannot be directly computed from OFV data. Since S expresses the ratio of tangential and axial momenta, an analogous, simplified descriptor can be defined as the ratio of x and y projected velocity components, where x is the projected radial coordinate and y is the axial coordinate. Thus, the simplified measure of flame swirl analogous to the swirl number is computed as follows.

$$S_v = \left| \frac{v_x}{v_y} \right|. \tag{7}$$

S_v was also computed in the interrogation areas shown in Figure 4 as the ratio of local mean x and y velocities. Figure 7 shows the extracted results for the swirl, CO_2 decreasing and increasing scenarios.

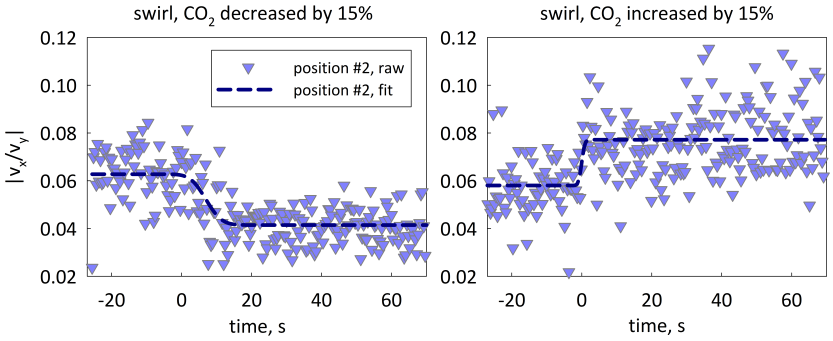

Fig. 7 The transient behavior of the simplified indicator of flame swirl, S_v, for the scenarios in which flame swirl was expected to change. The change of swirl was only significant in the upstream regions of the flames, therefore only the transient signals extracted in position #2 are shown. As expected, decreasing CO_2 co-flow decreased swirl, while increasing CO_2 co-flow increased swirl. Fit functions are of the logistic form.

As is apparent from Figure 7, decreasing CO_2 co-flow decreased the swirl of the flame, while increasing CO_2 increased it. This is in agreement with the OF velocity data (see Figure 6). Note that the flame spread caused by the increased tangential pull is not directly visible in the images due to the limited optical access. However, by looking at Figure 3, some widening is visible in the case of the CO_2 increasing scenario. This is most apparent when comparing the flame images of the CO_2 increase case with the CO_2 decrease case.

4 Remarks

In this section, various issues regarding the physical meaning of OF velocities and the practical applicabiity of the method are addressed.

4.1 Interpreting OF velocities

Section 3 demonstrated the responsiveness of OFV measurements to changes in operating conditions. However, it is important to point out that OF velocity, as it is extracted from typical line-of-sight images, is not equivalent to either flame front velocity, gas velocity or particle velocity. It is practical to consider OF velocity as a quantifier of the apparent, projected motion of scalar fields. The practicality of this consideration lies within the terms used to describe OF velocities:

1. The apparent nature of the motion suggests some subjectivity in OF velocity extraction. The most well-known cause of this subjectivity is the aperture problem - in other words, flow patterns close to occlusions and within bounded regions cannot be exactly determined. More generally, OF motion is always an approximation of the projected physical motion, as physical motion is not necessarily correlated to image intensity. Other difficulties contributing to the subjectivity of OF velocity are summarized in (Beauchemin and Barron 1995).
2. The nature of the projection responsible for image formation is a significant factor contributing to the uncertainty in the definition of OF velocities. When monitoring combustion systems, the image formation process typically includes emission, absorption and refraction. The emission of photons happens in a volume. The emitted photons interact with parts of the flame and some are absorbed. Since turbulent flames often exhibit steep gradients in their corresponding physical fields, the effect of absorption through flame layers is not constant over an image. This results in images in which it is unclear which layer of the flame is visible at a particular location, thus OF velocity maps are heavily convoluted by the effects of unknown observed depth. OF velocities may be more meaningful in the case of certain flame geometries than in others. Refraction plays a role in bending light rays that travel within the flame and through lenses. Image distortion caused by either excessively high gradients in the refractive index field of a flame or lens distortion affects the fidelity of obtained OF velocity values.
3. The emitting scalar field itself heavily determines what becomes apparent in images. When studying luminous flames, the scalar field is typically a function of local temperatures and the concentration of gaseous species and soot. In images of complex flame geometries, particularly of hollow flames surrounded by strongly absorbing layers, the extracted OF velocities mostly express the projected motion of the surface of the flame, possibly convoluted by a significant z-component of the velocity. It is thus important to know the practical limitations of OFV monitoring in terms of flame sizes and geometries. As the scalar field is a function of temperature and concentration, in some cases insufficient signal levels cause regions of missing data in OF velocity maps.

4.2 Sensitivity to input parameters

One way to assess the uncertainty caused by the subjectivity inherent in OF velocity extraction is measuring the sensitivity of the obtained data to the variation of the input parameters of the OF algorithm. The effect of input parameter variation were assessed by Monte-Carlo simulations. The simulations consisted of running the OF algorithm over a subset of flame images with input parameters drawn randomly from uniform probability distributions. The varied parameters were α, the relative importance of image intensity and γ, the relative importance of image gradients. The ranges of variation were 80-120 and 1-5, respectively. These ranges were determined empirically, by observing the extremes of the parameter combinations that still produced meaningful apparent motion fields. Each image was processed with a10^3 combinations of α and γ drawn from the ranges given above. The sensitivity of OF velocities to input parameter variation is expressed as the standard deviations of the populations of the 10^3 OF velocity values obtained at every pixel. The averages of these standard deviations over every image are shown in Figure 8. The subsets of images were picked from image sets of steady operation (see Table 2). A subset of 100 images were selected from cases with the co-axial burner and the swirl burner (total of 200 images).

As seen in Figure 8, the variation caused by OF velocities by the input parameter variation was generally higher in the case of images of the swirled flame. This alone does not tell much about the geometry of the flame - it merely implies that the motion of visual patterns arising in the swirled flame was more ambiguous than of those in the co-axial flame. The relative sensitivity of the y-component (vertical component) of OF velocities stayed under 5% in both the co-axial and swirl cases. The horizontal component showed a higher relative sensitivity, possibly because of the lower and zero-mean projected tangential velocities. The relative sensitivity of the vertical (projected axial) velocity component is promising.

4.3 Handling missing data

As mentioned in Section 4.1, the peculiarities of the emitting scalar field may yield insufficient image intensity (signal strength) either locally or globally in a flame image used to extract OF velocity. Images of inherently non-luminous or lifted flames, such as the ones shown in Figure 3, may contain featureless regions.

UU IR Author Manuscript

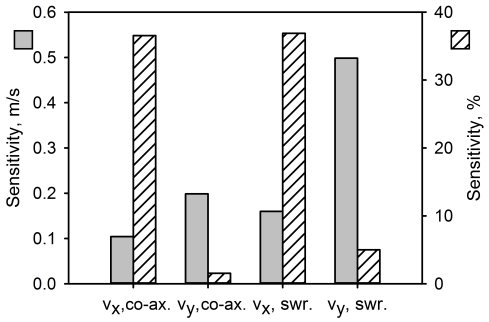

Fig. 8 The sensitivity of OF velocities to variations in parameters α and γ. Sensitivity is expressed as the standard deviation of OF velocity values computed in Monte-Carlo sets varying α and γ. The left vertical axis shows sensitivity in m/s units, while the right vertical axis shows sensitivity values relative to mean OF velocities.

"Holes" in intensity images can be treated statistically via forms of temporal averaging and missing data handling. Another method is to shift the range of imaged wavelengths to regions in which the monitored flames show sufficient luminosity. Sooting flames typically emit in the visible band, as demonstrated in Section 3. Non-sooting flames may still be monitored by the OFV technique in the infrared. Figure 9 shows synchronized pairs of visible and mid-wave infrared (MWIR) flame images along with axial profiles of OF velocity extracted from both visible and infrared image sequences.

For acquiring the infrared images shown in Figure 9, a FLIR SC6703 type MWIR camera was used. This camera responded to infrared light in the 3800-4000 nm wavelength range and was equipped with a 50 mm focal length MWIR lens. At a standoff of approximately 4 m, the system realized a magnification of 0.015 and a lateral resolution of 5 mm in the center plane of the flame. The size of the acquired MWIR images was 576×52, which roughly corresponded to a FOV of 9×100 cm^2. This camera was used in conjunction with the high-speed visible camera described in Section 2.2 in order to acquire synchronized pairs of visible and infrared images. The image pairs were spatially referenced by using multi-modal intensity registration that maximized the cross-correlation metric.

The cameras were triggered using the same dual-framing timing scheme as described in Section 2.2. The interframe time between frames within pairs was 1 ms. 10 frame pairs were acquired each second. The integration time of each frame was 60 µs.

Figure 9 demonstrates that by shifting the imaged spectral region, it is possible in certain cases to extract information from image regions that are featureless in the visible range. Imaging in MWIR may provide better OFV data in cases of non-sooting flames or flames with non-sooting regions, provided that in these regions, there is a sufficient concentration of hot hydrocarbons that emit in the infrared. The detached flames studied in this paper fall in this category. Figure 9 shows results obtained from images of a detached, unstable flame produced in the oxy-coal combustor described in Section 2.1. The axial velocity profile shows a local minimum of OF velocity around 0.27 m downstream of the burner. The location of this minimum approximately corresponds to the zone of ignition.

4.4 Performance

Performance was studied by profiling the GPU implementation of the OFV algorithm (Brox et al 2004) with the acquired flame images. The computational platform was an inexpensive personal computer with a CUDA-capable GPU. The obtained frame rates for typical flame images when computing the full OF velocity field were between 20 and 60 frames per second. When subsampling the images to define specific interrogation areas, the processing speed was up to two orders of magnitude faster. This performance is possibly sufficient for on-line applications. The time needed for image acquisition or the communication overhead between the camera and GPU was not included in the computation. At typical bus speeds of 100 MB/s and typical bitmap sizes of 0.05-1 MB (8-bit grayscale), the performance drop can be estimated to be 5-10% due to data transfer relative to the reported values, assuming direct copying to/from host memory.

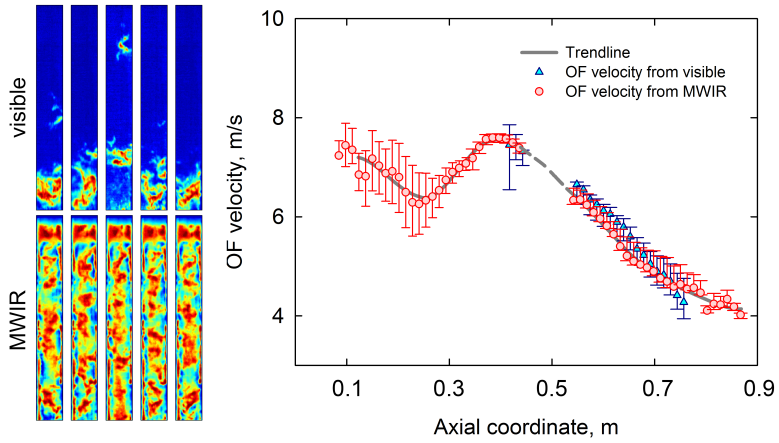

Fig. 9 Shifting the imaged wavelength band from the visible to the infrared may solve the problem of dark or partly featureless images in certain cases. The left side shows synchronized pairs of visible and MWIR images. Each column of two images is a synchronized pair - correspondence may be easier to recognize in regions where there is visible emission. The images were enhanced by adaptive histogram equalization (Pizer et al 1987) to improve the visibility of features. The right side shows axial profiles of OF velocity extracted from both the visible and MWIR image sequences. Error bars indicate the sensitivity of OF velocity values as described in Section 4.2. Uncertainty is increased in regions with lower contrast and/or less defined visual patterns. The dashed part of the trendline is interpolation between image areas which are occluded by the gap between the two pieces of the quartz window (see Section 2.2).

4.5 Practical considerations

As shown, the performance of the OFV method suggests potential in industrial applications. With regard to the achievable physical robustness of the system, we point out that a dedicated high-speed camera is not an absolute necessity for optical flow measurements under typical industrial conditions. First, less expensive dual-framing CCD cameras can be used to capture subsequent image pairs. If such a camera is not available, it is also possible to synchronize two regular (synchronizable) video cameras so that their combination practically realizes dual-frame imaging. In terms of rugged and heat-resistant imaging optics, the large number of previous studies (Kurihara et al 1986; Shimoda et al 1990; Baldini et al 2000; Baek et al 2001; Lu et al 2004, 2005; Baeg et al 2005; Lu et al 2008; Jiang et al 2009; Smart et al 2010; Zhang et al 2011; Xiangyu et al 2011; Sun et al 2011; Lou et al 2011) suggests that such hardware is available. Soot blowers, rugged optics and cooling are potentially required for safe operation. Naturally, implementing an on-line version of the OFV setup described in this paper might cause some drop of thermal efficiency in the operated combustion system due to the required cooling and cleaning of the optics. On the other hand, in contrast with conventional industrial methods for velocity measurement in pulverized-coal combustion systems (e.g., electrostatic correlation probes (Xu et al 2009) or pitot-tubes), the OFV technique is comparatively non-intrusive and can provide a characterization of apparent velocities in the full FOV, while being more robust than existing optical diagnostics methods that are conventionally used for velocimetry. Analyzing the economic feasibility of the technique is not part of the scope of this paper.

5 Conclusion

In this study, we examined the potential of utilizing the optical flow velocimetry (OFV) technique in the field of pilot-scale oxy-coal combustion and burner control. The main focus of this study was the assessment of the responsiveness and usefulness of optical flow velocity information in potential control and flame monitoring applications. A small, pilot-scale, oxy-coal combustion system was used to demonstrate the capabilities of the OFV technique. The transient velocity signals obtained during furnace operation showed promise in terms of responsiveness to system inputs. The obtained transient velocity data were consistent with physical intuition and the data of gas analyzers. The possible shortcomings of OFV, including the subjectivity and uncertainty in the extracted information, were listed. Mid-wave infrared imaging was proposed as a possible method for solving the problem of insufficient image intensity or signal strength that may be present in

certain images. Lastly, based on off-line performance tests, it was found that the computational efficiency of the OF algorithm used in this work was sufficient for the suggested applications.

6 Acknowledgment

The authors are thankful to Taylor Geisler (University of Utah) for assistance in pilot-scale tests and to Prof. Philip Smith (University of Utah) for his insights on interpreting the results. This material is based upon work supported by the Department of Energy under Award Number DE-NT0005015. The views and opinions of authors expressed herein do not necessarily state or reflect those of the United States Government or any agency thereof. This work was partially sponsored by the TAMOP-4.2.1.B-10/2/KONV-2010-0001 project with support by the European Union, co-financed by the European Social Fund. This research was carried out in the framework of the Center of Excellence of Sustainable Resource Management of the University of Miskolc.

References

Arik EB, Carr J (1997) Digital particle image velocimetry system for real-time wind tunnel measurements. In: International Congress on Instrumentation in Aerospace Simulation Facilities, pp 267–277

Baeg SY, Kim SM, Cho CH (2005) Development of flame monitoring system with optical receiver for pulverized coal firing boilers. In: Proceedings of SPIE 6041, ICMIT 2005: Information Systems and Signal Processing, pp 1–5

Baek WB, Lee SJ, Baeg SY, Cho CH (2001) Flame image processing and analysis for optimal coal firing of thermal power plant. In: Proceedings of the International Symposium on Industrial Electronics, vol 2, pp 928–931

Baldini G, Campadelli P, Lanzarotti R (2000) Combustion analysis by image processing of premixed flames. In: Proceedings of the International Conference on Image Processing, vol 2, pp 708–711

Beauchemin SS, Barron JL (1995) The computation of optical flow. ACM Computing Surveys 27(3):433–467

Bouguet JY (2000) Pyramidal implementation of the Lucas Kanade feature tracker - description of the algorithm. Tech. rep., Intel Corporation

Brox T, Bruhn A, Papenberg N, Weickert J (2004) High accuracy optical flow estimation based on a theory for warping. In: Proceedings of the Eighth European Conference on Computer Vision, pp 25–36

Buhre BJP, Elliott LK, Sheng CD, Gupta RP, Wall TF (2005) Oxy-fuel combustion technology for coal-fired power generation. Progress in Energy and Combustion Science 31(4):283–307

Cleveland WS (1979) Robust locally weighted regression and smoothing scatterplots. Journal of the American Statistical Association 74(368):829–836

Deriche R, Kornprobst P, Aubert G (1995) Optical-flow estimation while preserving its dis-continuities: a variational approach. In: Proceedings of the Second Asian Conference on Computer Vision, vol 2, pp 290–295

Farneback G (2001) Very high accuracy velocity estimation using orientation tensors, parametric motion, and simultaneous segmentation of the motion field. In: Proceedings of the Eighth International Conference on Computer Vision, vol 1, pp 171–177

Fielding J, Long MB (2000) Comparison of particle image velocimetry and optical flow velocimetry for turbulent flows and flames. In: Laser Applications to Chemical and Environmental Analysis - Combustion Diagnostics II

Fielding J, Long MB, Fielding G, Komiyama M (2001) Systematic errors in optical-flow velocimetry for turbulent flows and flames. Applied Optics 40(6):757–764

Gonzalez RC, Woods RE (2001) Digital Image Processing, 2nd edn. Prentice Hall

Gonzalez-Cencerrado A, Pena B, Gil A (2012) Coal flame characterization by means of digital image processing in a semi-industrial scale pf swirl burner. Applied Energy 94:375–384

Jiang ZW, Luo ZX, Zhou HC (2009) A simple measurement method of temperature and emissivity of coal-fired flames from visible radiation image and its application in a cfb boiler furnace. Fuel 88:980–987

Kurihara N, Nishikawa M, Watanabe A, Satoh Y, Ohtsuka K, Miyagaki M, Highashi T, Masai T (1986) A combustion diagnosis method for pulverized coal boilers using flame-image recognition technology. IEEE Transactions on Energy Conversion EC-1(2):99–103

Lou C, Li WH, Zhou HC, Salinas CT (2011) Experimental investigation on simultaneous measurement of temperature distributions and radiative properties in an oil-fired tunnel furnace by radiation analysis. International Journal of Heat and Mass Transfer 54:1–8

Lu G, Yan Y, Colechin M (2004) A digital imaging based multifunctional flame monitoring system. IEEE Transactions on Instrumentation and Measurement 53(4):1152–1158

Lu G, Gilabert G, Yan Y (2005) Vision based monitoring and characterisation of combustion flames. Journal of Physics: Conference Series - Sensors and their Applications 15:194–200

Lu G, Yan Y, Cornwell S, Whitehouse M, Riley G (2008) Impact of co-firing coal and biomass on flame characteristics and stability. Fuel 87:1133–1140

Pizer SM, Amburn EP, Austin JD, Cromartie R, Geselowitz A, Greer T, ter Haar Romeny B, Zimmerman JB, Zuiderveld K (1987) Adaptive histogram equalization and its variations. Computer Vision, Graphics, and Image Processing 39:355–368

Richards FJ (1959) A flexible growth function for empirical use. Journal of Experimental Botany 10(2):290–301

Roberts JW (2012) Control of underactuated fluid-body systems with real-time particle image velocimetry. PhD thesis, Massachusetts Institute of Technology

UU IR Author Manuscript

Scholz J, Wiersbinski T, Ruhnau P, Kondermann D, Garbe CS, Hain R, Beushausen V (2008) Double-pulse planar-lif investigations using fluorescence motion analysis for mixture formation investigation. Experiments in Fluids 45:583–593

Shimoda M, Sugano A, Kimura T, Watanabe Y, Ishiyama K (1990) Prediction method of unburnt carbon for coal fired utility boiler using image processing technique of combustion flame. IEEE Transactions on Energy Conversion 5(4):640–645

Smart J, Lu G, Yan Y, Riley G (2010) Characterisation of an oxy-coal flame through digital imaging. Combustion and Flame 157:1132–1139

Sun D, Lu G, Zhou H, Yan Y (2011) Flame stability monitoring and characterization through digital imaging and spectral analysis. Measurement Science and Technology 22:1–9

Xiangyu Z, Qiang C, Chun L, Huaichun Z (2011) An improved colorimetric method for visualization of 2-d, inhomogeneous temperature distribution in a gas fired industrial furnace by radiation image processing. Proceedings of the Combustion Institute 33:2755–2762

Xu C, Zhang J, Yang D, Zhou B, Tang G, Wang S (2009) Dense-phase pneumatically conveyed coal particle velocity measurement using electrostatic probes and cross correlation algorithm. Journal of Physics: Conference Series 147

Zhang J, Okerlund R, Eddings EG, Wendt JOL (2007) Ignition of axial pulverized coal jets in a specially designed 100kw oxy-fuel combustor. In: Proceedings of the 6^{th} International Symposium on Coal Combustion, pp 305–309

Zhang J, Kelly KE, Eddings EG, Wendt JO (2011) Ignition in 40 kw co-axial turbulent diffusion oxy-coal jet flames. Proceedings of the Combustion Institute 33:3375–3382

UU IR Author Manuscript